sensors

MDPI

Article

Skin Phototype Classification with Machine Learning Based on Broadband Optical Measurements

Xun Yu [1], Keat Ghee Ong [1,2] and Michael Aaron McGeehan [1,2,*]

[1] Department of Bioengineering, Phil and Penny Knight Campus for Accelerating Scientific Impact, University of Oregon, Eugene, OR 97403, USA; xunyu@uoregon.edu (X.Y.); kgong@uoregon.edu (K.G.O.)
[2] Penderia Technologies Inc., Eugene, OR 97403, USA
* Correspondence: mmcgeeha@uoregon.edu

Abstract: The Fitzpatrick Skin Phototype Classification (FSPC) scale is widely used to categorize skin types but has limitations such as the underrepresentation of darker skin phototypes, low classification resolution, and subjectivity. These limitations may contribute to dermatological care disparities in patients with darker skin phototypes, including the misdiagnosis of wound healing progression and escalated dermatological disease severity. This study introduces (1) an optical sensor measuring reflected light across 410–940 nm, (2) an unsupervised K-means algorithm for skin phototype classification using broadband optical data, and (3) methods to optimize classification across the Near-ultraviolet-A, Visible, and Near-infrared spectra. The differentiation capability of the algorithm was compared to human assessment based on FSPC in a diverse participant population (n = 30) spanning an even distribution of the full FSPC scale. The FSPC assessment distinguished between light and dark skin phototypes (e.g., FSPC I vs. VI) at 560, 585, and 645 nm but struggled with more similar phototypes (e.g., I vs. II). The K-means algorithm demonstrated stronger differentiation across a broader range of wavelengths, resulting in better classification resolution and supporting its use as a quantifiable and reproducible method for skin type classification. We also demonstrate the optimization of this method for specific bandwidths of interest and their associated clinical implications.

Keywords: Fitzpatrick skin type; K-means clustering; machine learning; skin optical properties; dermatology; skin type classification

Citation: Yu, X.; Ong, K.G.; McGeehan, M.A. Skin Phototype Classification with Machine Learning Based on Broadband Optical Measurements. *Sensors* **2024**, *24*, 7397. https://doi.org/10.3390/s24227397

Academic Editor: Benjamin L. Miller

Received: 20 October 2024
Revised: 15 November 2024
Accepted: 15 November 2024
Published: 20 November 2024

1. Introduction

Visual skin phototype evaluations are widely used in medicine. From clinical uses such as screening for skin cancer and skin grafting immunosuppression to cultural research in colorism and cosmetic product development [1–5], skin phototype classification continuously demonstrates usefulness across academic, clinical, and industrial applications [6]. In addition to these use cases, skin phototype classification enables clinicians to assess tissue health to diagnose and/or treat medical conditions or risk thereof [3]. The Fitzpatrick Skin Phototype Classification (FSPC) scale (Figure 1a) was developed in 1975 to classify different skin phototypes according to their susceptibility to sunburn and skin cancer in response to ultraviolet (UV) radiation [7]. Despite its broad adoption for clinical use, the FSPC has become controversial in recent years for its underrepresentation of populations with darker skin pigmentation, poor classification resolution (i.e., limited to only six possible phototypes), and subjective nature rather than quantifying skin type through empirical evidence or measurement tools [8]. The FSPC scale also has a major limitation in its reliance on human visual data extracted from the relatively narrow visible light (VL) spectrum as inputs, which may not represent skin optical responses to UV radiation as intended. Similarly, the FSPC has limited use for clinical conditions that are not UV-sensitive, such as skin optical properties in the infrared and near-infrared spectra, which may hold significance for classifying skin phototypes for other clinical applications (e.g., personalized

and optimized exposure dosage and wavelengths for photobiomodulation therapy) [9]. Furthermore, the FSPC is sometimes misused to categorize race and ethnicity rather than its intended use with UV exposure risks [10]. Each of these compounding factors limits the clinical usefulness of the FSPC and highlights a need for a quantitative and repeatable skin type classification system that can probe skin optical properties at specific optical bandwidths of interest to target specific clinical uses.

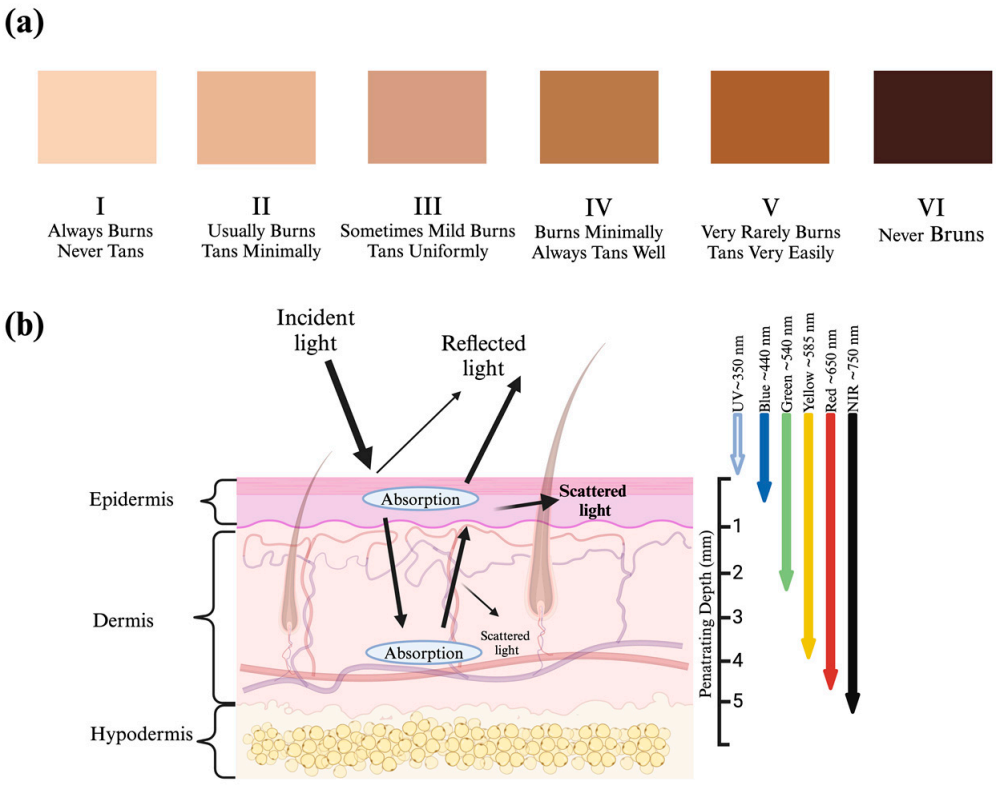

Figure 1. (**a**) Fitzpatrick Skin Type Scale (I–VI) and (**b**) Generalized penetration depths of various wavelengths of light through tissue structures of interest [11].

The limitations of visual chromatic skin evaluations, such as the FSPC, may have detrimental impacts on patient care, such as misleading clinicians, causing delay or deviation from optimal treatment procedures [12]. For example, inaccurate blood oxygenation measurements have been documented among patients with darker skin types compared to those with lighter skin types, increasing the possibility of undiagnosed hypoxemia [12–14]. Specifically, one meta-analysis reported a mean overestimation of 1.11% and 1.52% of arterial and peripheral blood oxygenation in people with high levels of skin pigmentation [12]. Moreover, patients with highly pigmented skin are subject to higher risks of undiagnosed bacterial-laden wounds based on the FSPC evaluation, leaving darker skin phototype patients at higher risk for disease progression [15]. In a review of racial disparities in dermatology, patients with dark skin phototypes were less likely to receive a variety of pharmaceutical interventions needed for dermatological care and, thus, more likely to have more severe dermatological disease progression [16]. Finally, questionnaire-based skin type classifications, such as the FSPC, are shown to overestimate pigmentation among subjects with light skin and underestimate pigment for those with dark skin, highlighting a need for a more representative skin phototype scale with more quantitative and reproducible classificational approaches based on skin optical properties instead of appearances [17,18].

Past research efforts have explored different sensor-based methods, such as colorimeters and spectrophotometers, in combination with algorithms such as the Individual Typology Angle (ITA) [19] and International Commission on Illumination L*a*b* color space (CIELAB) [20,21], or surveys to quantify and classify human skin types [22]. These ap-

proaches use one or multiple light sources to emit standardized or distributed wavelengths, allowing photodetectors to measure light reflected or transmitted through tissue [23]. Light intensity data are then used as algorithm inputs to assess skin optical characteristics. In the 3-dimensional CIE L*a*b* model, L* represents luminescence, a* measures red/green balance, and b* measures yellow/blue balance [23]. The ITA algorithm similarly models luminance, yellow, and blue light intensities as an arc, classifying skin phototypes based on angle ranges. While CIE L*a*b* and ITA offer more repeatable and quantitative measurements than visual assessments (e.g., the FSPC Scale), they are limited by narrow visible bandwidths and cannot be used to analyze high-dimensional optical data. This limits their ability to distinguish between spectral features with similar appearances [23]. Additionally, these algorithms rely on wavelength intensity ratios rather than raw irradiance values, potentially reducing sensitivity to specific physiological features and differentiation between skin types.

Different wavelengths of the incident light penetrate different tissue depths and structures (Figure 1b) [24]. For example, longer visible wavelengths, such as red light (~650 nm), penetrate deeper than shorter wavelengths, such as blue light (~450 nm). Thus, optical resonance at these wavelengths represent different anatomical and physiological features of the tissue [11,24]. Previous research investigating tissue penetration depths using different wavelengths via computational simulations [24,25] and observations from photobiomodulation Therapy (PBMT) [26] suggests that nonuniformity in tissue structures, thickness, and optical properties (i.e., absorption and scattering coefficients) [27] all contribute to difficulties in creating standardized qualitative or quantitative tools to classify skin types. Machine learning algorithms, however, show promise for aiding in skin type classification. In one study, machine learning tools aided clinicians in improving skin disease diagnosis accuracy by more than 33% compared to clinicians alone [28]. This promising result underscores the potential of machine learning algorithms in aiding dermatological care, offering new options for a more accurate and equitable future. However, the same study reported that the machine learning approach still struggled to accurately diagnose skin diseases in darker skin phototype patients based on the FSPC scale [28].

Classifying skin phototypes across diverse populations is challenging due to complex anatomical variability, differing tissue absorbance properties, and varied optical responses to broad-spectrum light. These challenges are further complicated by a mismatch between the salient optical properties of distinct skin structures, which are dynamic in response to broad-spectrum light spanning from UV to IR, in contrast to human vision, which operates in visible spectra [29]. At the cutaneous level, visual perception of skin color is affected by physical phenomena such as light scattering, absorption, and penetration depth within different skin layers (Figure 1b) [27]. It has been reported that 4–7% of a near-normal incident beam of light between 200–3000 nm is reflected away from the skin's surface, or stratum corneum, regardless of skin type [27,30]. The remaining 93–96% of incident light is absorbed or refracted at the epidermis and dermis layers [31]. Melanin blocks UV light [32] and exists in two forms: pheomelanin (yellow-brown) and eumelanin (black-brown) [33,34]. Eumelanin is more abundant in the epidermis of individuals with darker skin types [35]. Despite efforts to correlate pigmentation, skin optical properties, and the FSPC scale, human color vision is most sensitive to blue, green, and red light spectra [23]. These narrower wavelengths do not fully account for the complex optical properties of human skin, which span the full photo spectrum. For example, melanosomes, a type of organelle in pigment cells, are reported to have scattering effects orders of magnitude higher than melanin's absorbing effects across the Visible Light (VL) and Near-Infrared (NIR or Near-IR) spectra at 400–1,600 nm [35]. In contrast, melanin accounts for 50–75% of light absorption in the UV spectrum, leaving less light reflected in this spectrum among individuals with skin that contains high melanin concentration [36]. The complex optical properties of human skin, shortcomings of visual chromatic evaluations, and limitations in previous sensor-based work highlight an ongoing need for a more robust, objective skin phototype classification method with UV, Visible, and Near-IR spectra considerations. Such

a method will provide a quantitative and repeatable framework for evaluating complex skin optical properties, thus yielding better diagnostic reliability and repeatability.

Here, we report an objective sensor-based skin optical properties classification approach that characterizes and classifies different skin phototypes based on optical similarities via a machine learning algorithm (K-means clustering) [37] across a 410940 nm spectral dataset for a culturally diverse subject pool. Historically, K-means classification models have been used as medical image classifiers for skin cancer detection and detection of human skin and gestures [38,39]. Based on computational simplicity and the ability to evaluate high-dimensional feature spaces, K-means clustering is a good candidate algorithm for evaluating and grouping sensor-derived broad-spectrum skin optical properties from diverse human populations. This proposed integrated sensor and algorithm approach serves not only to provide a framework for an objective, repeatable, and reliable skin type classification but also to further the understanding of the relationships between visual skin evaluations and underlying skin optical properties.

2. Materials and Methods

2.1. Participants

Thirty participants (16 females and 14 males) participated in this study. This cohort spanned an even distribution of the entire FSPC scale I–VI (five participants per category, Table 1). All enrolled participants were free of cardiopulmonary or respiratory disease. Table 1 summarizes participant demographic and anthropometric information. All research activities were approved by the University of Oregon Institutional Review Board, and written consent was obtained from all participants prior to the experiment.

Table 1. Summary table of participant demographic and anthropometric information.

FSPC Scale	Numbers of Participants	Age (Years) (Mean ± SD)	Biological Sex	Self-Identify Ethnicity
Type I	5	23.4 ± 5.78	M: 2 F: 3	White: 5
Type II	5	24.7 ± 6.00	M: 3 F: 2	Asian: 2 Hispanic: 1 White: 2
Type III	5	23.0 ± 4.41	M: 2 F: 3	Asian: 5
Type IV	5	22.4 ± 3.65	M: 3 F: 2	Asian: 1 Black: 4
Type V	5	23.9 ± 4.99	M: 4 F: 1	Asian: 1 Black: 4
Type VI	5	23.8 ± 5.05	M: 0 F: 5	Black: 5

SD: Standard deviation.

2.2. Experimental Overview

The experimental flow is illustrated in Figure 2. Participants first completed a questionnaire where they self-reported their age, biological sex, and ethnicity (Table 1). A trained research team member then evaluated the participants' skin on the FSPC scale under standardized lighting conditions (lux: 967 lux, color temperature: 3442 K, confirmed by a spectrometer (Light Master IV, OPPLE, Shanghai, China). Skin was evaluated from the back of the hand between the thumb and index finger. This anatomic landmark was selected as the evaluation site for its typical skin uniformity, lack of hair, and unobtrusive access. Skin type was evaluated by comparing the skin color to the FSPC scale displayed on an OLED computer monitor presented in the same field of view. Left vs. right hand selection was randomized between participants.

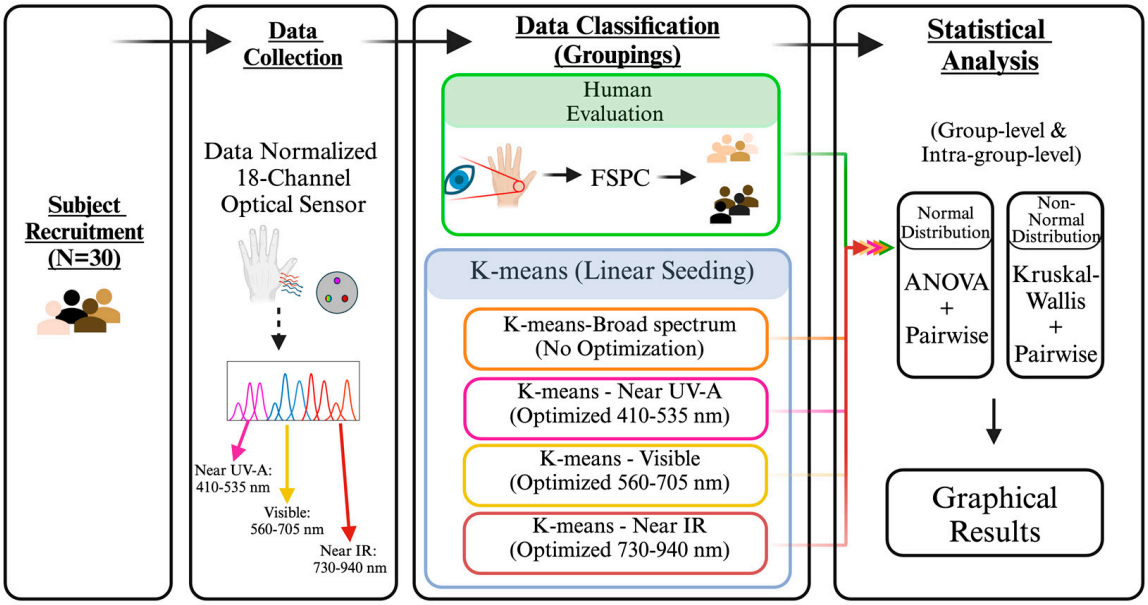

Figure 2. Block diagram of experimental procedures.

After visual skin classification, participants underwent skin optical properties measurements with the spectral sensor (Section 2.3). The sensor was placed, contacting the participant's skin at the same anatomic landmark as visual evaluations. Light pressure was applied to the sensor to isolate it from environmental light but not cause discomfort for the participant. Ten repeated samples were collected from each sensor (AS7261, 2, and 3), which measure irradiance at the Near-UV-A, Visible, and Near-IR spectra. In total, 180 data points (ten data points per channel across 18 channels) were collected for each participant; 16-bit data were transmitted to a PC via serial communication for subsequent processing (Section 2.4). Classification methods (FSPC vs. K-means) were then compared for their ability to differentiate skin phototypes (Section 2.5). The purpose of this study was to independently evaluate the FSPC and K-means methods for their ability to differentiate skin phototypes. The FSPC method was not considered the ground truth, and thus, direct comparisons for K-means vs. FSPC accuracy were not made.

2.3. Sensor Design

The optical spectroscopy sensor (Figure 3) consists of spectrum-paired light-emitting diodes (LEDs) and photodiodes designed to probe the optical properties of skin. Three LEDs (Luxeon 3014, Lumileds, San Jose, CA, USA; VLMU3100, Vishay Semiconductors, Shelton, WA, USA; SIR19-21C/TR8, Everlight Electronics; New Taipei City, Taiwan) emit light spectra at 385–425 nm, 425–725 nm, and 780–950 nm bandwidths, respectively, spanning the Near-UV-A to Near-IR spectra. By combining three spectrophotometry sensors (AS72651, 2, and 3, AMS, Premstatten, Austria) with six bandpass filters each, the platform measures light resonance at 18 discrete wavelengths ranging from 390 nm to 960 nm with a sensitivity of 28.6 nW/cm^2 of irradiance. The platform produces 16-bit digital irradiance values (range: 0–2^{16}) at each wavelength via I2C communication for objective spectral characterization with data rates up to 400 kbit/s. Custom circuitry and firmware (C++, Visual Studio, Microsoft, Bellevue, WA, USA) on a microcontroller (WRL-15484, SparkFun, Niwot, CO, USA) controls the sensors and transmits data via serial connection to a PC for subsequent analysis. A 3D-printed (Prusa, Newark, DE, USA) Polylactic acid (PLA) sensor housing was designed to isolate the sensor from ambient light and allow measurements at specific spectra (i.e., Near-UV-A, Visible, or Near-IR) if desired.

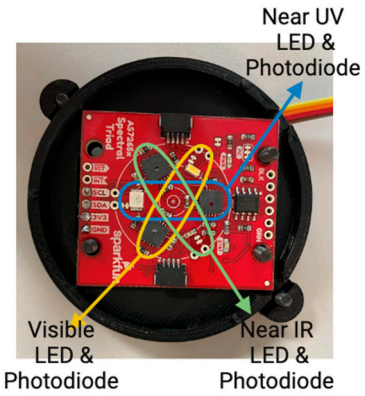

Figure 3. Sensor outside of packaging showing electronics, LEDs, and photodiodes.

2.4. Data Processing

Raw data from all participants were imported and processed in MATLAB R2023b (MathWorks. Inc, Natick, MA, USA). A broad description of the processing procedures is provided in Section K-Means Classification and Custom Seeding. An average irradiance value for each channel was calculated for each participant as the mean of the ten samples collected at each channel. Each channel's data were then normalized to the maximum measurement observed in that channel, mapping each wavelength's dataset on a 0 to 1 scale. The normalized participants' measurements were then grouped based on the FSPC category, hereafter referred to as "human evaluation" in statistical comparisons or used as inputs to the K-means clustering algorithm (Section K-Means Classification and Custom Seeding) (Figure 2).

K-Means Classification and Custom Seeding

The K-means clustering method (Figure 4) is a commonly used data classification approach that partitions data points into mutually exclusive clusters/groups (i.e., skin phototype) based on similarities in observed characteristics (i.e., irradiance measurements). This clustering method was selected for its simple mathematics, low computational power requirements, easily interpreted results, and comprehensive documentation in an effort to enhance clinical interpretation compared to more ambiguous black-box machine learning approaches. In this experiment, all 30 participants' data were mapped in an 18-dimensional feature space, with each dimension representing the skin's optical properties measured at a specific wavelength. Data were partitioned into $k = 6$ clusters based on the number of categories in the FSPC scale. The classification results arising from the K-means method do not follow the same ranked order logic as the FSPC. Instead, K-means provides a cluster of participants with similar optical properties across a particular bandwidth of interest. However, clusters with high irradiance values in a particular bandwidth may not be high in another, and thus, the ranked order logic should not be applied to K-means results.

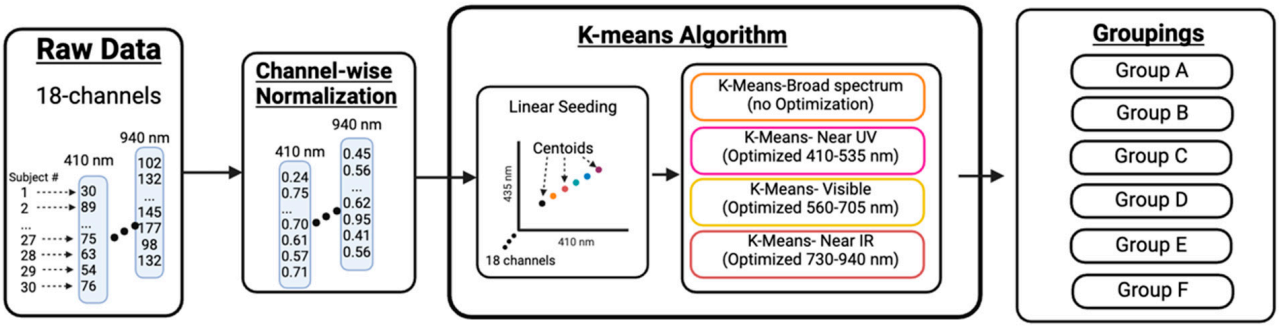

Figure 4. K-means classification workflow diagram.

The goal of this K-means classification approach is to find the six cluster centroid positions that best partition participants based on the least squares Euclidean distance of each data point to the centroid. The algorithm also seeks to maximize the Euclidean distance between centroids (i.e., maximize differentiation between groups). As such, initial centroid positioning can influence the ultimate classification results. In this study, randomly assigned centroid locations are not appropriate due to the nonnormal distribution of the data across 18 wavelengths. Moreover, the six centroids should not be initialized at the average irradiance value (or center of the domain) of each wavelength to avoid introducing wavelength weighting bias, which would skew classification results based on the wavelength with the highest irradiance value. To avoid these pitfalls, we utilized a custom centroid seed function whereby the centroids were initialized at evenly distributed positions along a linear function spanning the full irradiance range (minimum to maximum) observed at each wavelength. This approach provides a repeatable initial position for each centroid spanning the full range of irradiance values present in the dataset, reduces the chance of convergence at false local minima, and avoids introducing bias due to unequal irradiance values at different wavelengths.

To fully explore the classification capability of the K-means algorithm, four K-means analyses were performed. K-means$_{410–940}$ (Broad-spectrum) used all 18 wavelengths as grouping criteria and categorized participants based on skin optical properties across the full bandwidth of light tested. K-means$_{410–535}$ used six wavelengths ranging from 410–535 nm as grouping criteria and evaluated groupwise similarities across the Near-UV-A and lower visible spectra. Similarly, K-means$_{560–705}$ and K-means$_{730–940}$ used six wavelengths ranging from 560–705 nm and 730–940 nm, respectively, as grouping criteria to partition subjects across Visible and Near-IR spectra. By segmenting these spectra, we demonstrated this approach can be optimized for categorizing participant skin types based on specific bandwidths of interest and their associated clinical applications. For example, UV sensitivity with K-means$_{410–535}$, skin chromatic appearances with K-means$_{560–705}$, or therapeutic wavelength identification with K-means$_{730–940.}$ Additionally, this approach highlights that participants with similar skin types in a particular bandwidth are not necessarily similar at other bandwidths, demonstrating the need for customizability based on different clinical needs.

2.5. Statistical Analysis

In total, five classification grouping results (one human evaluation-classified dataset and four K-means-classified datasets) were individually investigated for their ability to classify skin type based on skin optical properties across the wavelengths tested. All statistical tests were performed in GraphPad 10 prism (GraphPad Software Inc., Boston, MA, USA). Each dataset was first tested for normality via the Shapiro-Wilk normality test ($\alpha = 0.05$). If the normality assumption was met, the classification methods' main effects of grouping on irradiance values were tested using one-way ANOVA analyses ($\alpha = 0.05$) at each wavelength. If the normality assumption was violated, the nonparametric Kruskal–Wallis test (K-W) ($\alpha = 0.05$) was used to evaluate the main effects. For all analyses, post-hoc pairwise comparisons were performed via Tukey's Honest Significant Differences (HSD) tests (ANOVA) and Dunn's method (K-W) with adjusted *p*-values to evaluate the resolution of the classification methods (i.e., the ability to differentiate between groups at each wavelength). Pairwise comparison *p*-values are reported in Appendix A.

An average Silhouette value [40] was also calculated for each cluster to quantify the quality of clusters generated by each K-means approach and FSPC evaluation. The Silhouette value is calculated as the difference between intra- and inter-cluster distances (average distance of a point to all other data points from the same cluster and average distance of this point to all other data points in the next nearest cluster, respectively) normalized to the maximum value of each. Silhouette values range from -1 to 1, with higher scores indicating better clustering quality.

3. Results and Discussion

3.1. Clustering Results

Thirty subjects were classified based on four methods, and their respective grouping results were subsequently analyzed (Sections 3.2 and 3.3). As shown in Table 2, the 30 subjects evenly covered the six skin phototypes of the FSPC scale based on human evaluation (n = 5 per FSPC group). However, based on skin optical data measured by the sensor, the K-means classification method grouped subjects nonuniformly across six categories. Moreover, in each of the K-means approaches, except K-means$_{410–535}$, there were outlier groups in which one or more clusters contained only one participant. This occurs due to the lack of similarities with other subjects from the pool and may be explained by three causes: (1) the sample size is too small that no other subjects share similar optical properties with the outlier; and/or (2) k = 6 clusters is a suboptimal target for grouping (i.e., actual skin phototypes are more or less numerous than the FSPC); and/or (3) the evenly distributed channel-wise weight enlarged the differences between subjects that share similar optical properties. It is also important to note that there is no one-to-one matching relationship between the grouping results of human evaluation and K-means classification methods. It is important to note that for the purposes of this study, the FSPC scale was not regarded as the ground truth for classifying skin phototypes. Hence, there is no basis for comparison between methods for group size or accuracy. All classification results should be considered independent from one another. Groups with n = 1 were excluded from the statistical analysis.

Table 2. Summary table of grouping results for human evaluation and K-means classification.

Human Evaluation		K-means Classification				
Skin Types	Subject Counts	Clusters	Subject Counts			
			Broad-Spectrum	Near-UV-A	Visible	Near-IR
Type I	5	Group A	3	3	7	4
Type II	5	Group B	9	5	4	11
Type III	5	Group C	12	6	13	6
Type IV	5	Group D	4	10	3	5
Type V	5	Group E	1	2	1	1
Type VI	5	Group F	1	4	2	3

The Silhouette values (SV) varied based on different clustering approaches (Table 3). Overall, the K-means$_{410–940}$ resulted in the highest average SV (0.245 ± 0.358), with the FSPC Human Evaluation and K-means$_{730–940}$ producing the lowest average SVs (-0.084 ± 0.387 and -0.088 ± 0.263). Clusters with SVs < 0.25 indicate low quality of data clustering (i.e., failure to identify and differentiate the distinctive optical features encoded within different skin types). In contrast, 0.25 < SV < 0.50 indicates weak-to-moderate quality, and SV > 0.50 indicates a cluster with high quality differentiation. Conditions with clusters with SV < 0.25 may indicate that k = 6 clusters is a suboptimal target. The K-means$_{410–940}$ produced three adequate-quality clusters and one low-quality cluster, indicating that broadband optical data clustered into three groups may be viable. Future work should seek to further explore the optimal target number of clusters for maximizing the quality of data classification.

Table 3. Summary of Silhouette values for the human evaluation and K-means approaches.

	Silhouette Values		
	Cluster Type	**Cluster Silhouette Value Mean ± SD**	**Method Silhouette Value Mean ± SD**
FSPC (Human Evaluation)	**Type I**	−0.540 ± 0.080	−0.084 ± 0.387
	Type II	−0.374 ± 0.180	
	Type III	0.197 ± 0.243	
	Type IV	0.117 ± 0.432	
	Type V	−0.090 ± 0.280	
	Type VI	0.189 ± 0.344	
K-means$_{410–940}$ (Broad spectrum)	**Group A**	0.547 ± 0.131	0.245 ± 0.358
	Group B	−0.212 ± 0.162	
	Group C	0.438 ± 0.178	
	Group D	0.488 ± 0.137	
	Group E *	—	
	Group F *	—	
K-means$_{410–535}$ (Near-UV-A)	**Group A**	0.561 ± 0.073	0.159 ± 0.321
	Group B	−0.069 ± 0.202	
	Group C	−0.135 ± 0.321	
	Group D	0.251 ± 0.190	
	Group E	0.621 ± 0.127	
	Group F	0.119 ± 0.248	
K-means$_{560–705}$ (Visible)	**Group A**	0.179 ± 0.148	0.040 ± 0.214
	Group B	0.169 ± 0.212	
	Group C	−0.039 ± 0.183	
	Group D	−0.007 ± 0.298	
	Group E *	—	
	Group F	−0.124 ± 0.306	
K-means$_{730–940}$ (Near-IR)	**Group A**	−0.237 ± 0.075	−0.088 ± 0.263
	Group B	−0.062 ± 0.212	
	Group C	−0.204 ± 0.266	
	Group D	−0.100 ± 0.191	
	Group E *	—	
	Group F	0.264 ± 0.461	

* Cluster contains only one subject; thus, a Silhouette value cannot be calculated.

3.2. Group-Level Analysis

As shown in Figure 5a, the human evaluation classification method resulted in statistically significant differences between skin types at only four wavelengths: 560 nm, 585 nm, 645 nm, and 705 nm, suggesting that humans rely primarily on these wavelengths when distinguishing skin types. However, the skin types differentiated at 705 nm failed to establish statistical significance when examined with pairwise comparison due to the lower adjusted *p*-value used (Section 3.3 and Appendix A). Moreover, the human classification method failed to establish significance from 410–535 nm, colors that span from blue to cyan. This observation aligns with previous research showing that human eyes are less sensitive to subtle differences from 390–500 nm spectra under the photopic condition [41] and more sensitive to distinguishing light in the yellow, green, and red spectra [41], which is also evident in the significant differences observed at 560 nm, 585 nm, and 645 nm in the human evaluation-classified condition (Figure 5a). This observation aligns with previous research showing that the trichromatic human photonic vision has a peak spectral sensitivity at approximately 555 nm, a combination wavelength from three types of short, middle, and long cone cells [42,43]. In summary, the chromatic assessment of the skin types via human evaluation only offers limited differentiation capability primarily constrained to a narrow bandwidth within the visible spectrum (560–645 nm) that leaves Near-UV-A and Near-IR spectrum unexplored.

While the results suggest that human evaluation-based classification relies primarily on visible light spectra for differentiating skin types, data from the K-means$_{410–940}$ (Figure 5b) show that the Near-UV-A and lower visible wavelengths provide the most differentiating power across the bandwidth tested. When compared to the human evaluation condition, the K-means$_{410–940}$ algorithm provided higher differentiation power, as shown in Figure 5b, showing statistical differences in an additional five wavelengths compared to human FSPC evaluations. More specifically, these additional wavelengths are typically found closer to the UV spectrum rather than the IR spectrum. This suggests that the actual

optical properties of the skin may be encoded within the Near-UV-A and lower visible (435–585 nm) range, while the Near-IR spectrum (730–940 nm) may primarily encode information about body temperature, making it unsuitable for skin type classification.

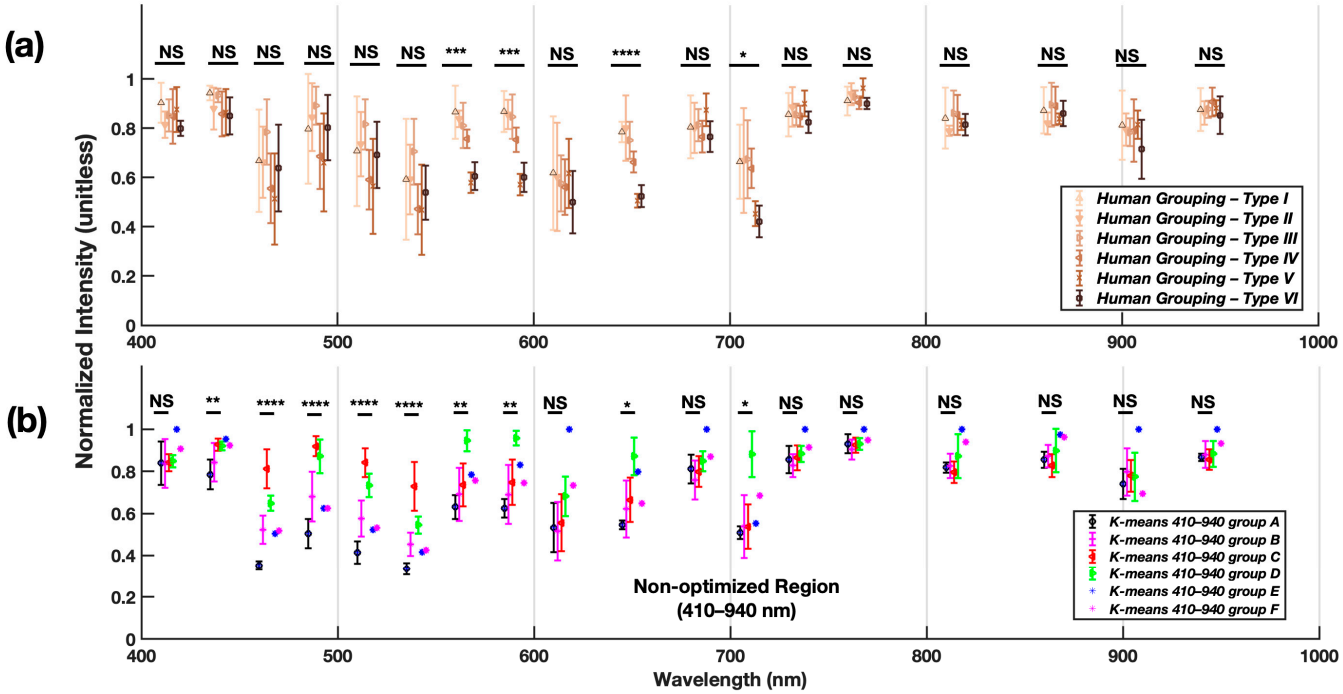

Figure 5. Normalized intensity of (**a**) human evaluation skin classification method vs. (**b**) K-means$_{410–940}$ across a broad spectrum bandwidth; Significant main effects ($\alpha = 0.05$) of the group on irradiance intensity are reported. NS: no statistical difference, *: $p < 0.05$, **: $p < 0.01$, ***: $p < 0.001$, ****: $p < 0.0001$. All group-level statistical values across different wavelengths can be found in Appendix A, Figures A1 and A2.

Figure 6 shows the optimized K-means classification results in which the algorithm was tuned to classify skin types based on the specific wavelengths of interest. Specifically, in Figure 6a, the K-means$_{410–535}$ algorithm was applied with centroids' seeding condition that focuses only on 410–535 nm and neglects other wavelengths. The results showed optimized dispersion in this spectrum specifically. This approach may have clinical significance for classifying skin phototypes for UV sensitivity rather than color (visible spectrum) or perfusion/temperature (IR spectrum). Similarly, desirable grouping results through visible spectrum optimization are shown in Figure 6b. In this approach, statistical differences were seen not only among the optimized wavelengths (560–705 nm) but also spanning further into part of the Near-IR (730–760 nm). In contrast to the clear and effective classification shown above in K-means$_{410–535}$ (Near-UV-A) and K-means$_{560–705}$ (Visible), the K-means$_{730–940}$ method (Near-IR) shown in Figure 6c resulted in less dispersion between the classification groups. Nevertheless, significant main effects of group on intensity were observed in five of the six optimized wavelengths. In combination, bandwidth optimization of the K-means classification method can better differentiate various skin types through the wavelength spectrum from 410–705 nm. The less concentrated statistical differences of the IR optimization results might be due to the normalized intensity obtained through the Near-IR spectrum encoding body temperature instead of actual reflective skin optical properties.

In summary, the K-means classification methods provided better skin optical-based classification across the 410–705 nm spectrum (i.e., differentiation across different skin types) when compared to human evaluation classification based on the FSPC scale. Optimization of K-means classification based on the spectra of interest, such as Near-UV-A or Visible, offers unique opportunities to tailor skin type differentiation towards various medical

applications. For example, the K-means method optimized on the Near-UV-A spectrum can be used to better assess the skin cancer risk among different groups of patients based on the skin's optical properties instead of the skin color alone [39,44]. K-means optimized at the visible spectrum can be used to better match the cosmetic appearance of a skin graft [45]. The IR spectra-focused K-means classification can be utilized in identifying optimal therapeutic wavelength in photobiomodulation [9].

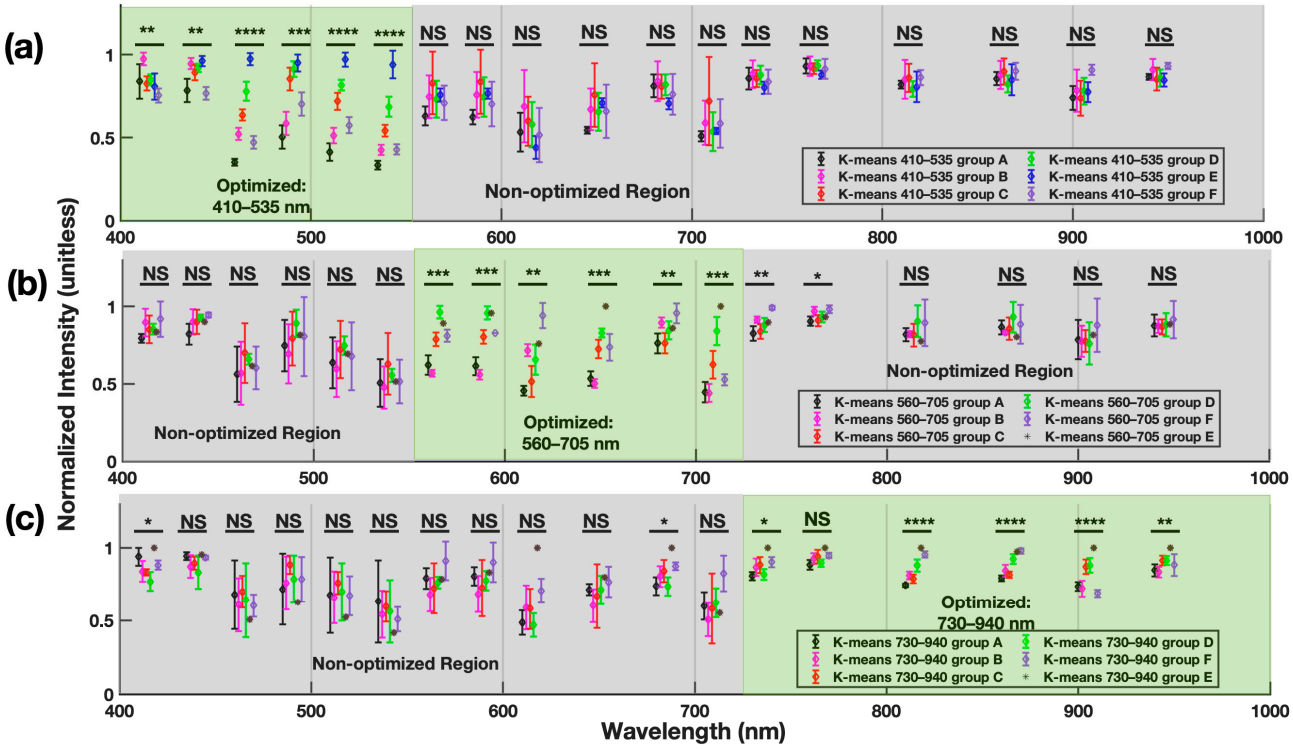

Figure 6. Normalized intensity of optimized (**a**) K-means$_{410–535}$, (**b**) K-means$_{560–705}$, and (**c**) K-means$_{730–940}$ across a 410–940 nm bandwidth. Green shading denotes optimized bandwidths in the K-means classification approach, whereas grey shading denotes neglected bandwidths. Significant main effects ($\alpha = 0.05$) of the group on irradiance intensity are reported. NS: no statistical differences, *: $p < 0.05$, **: $p < 0.01$, ***: $p < 0.001$, ****: $p < 0.0001$. All group-level statistical values across different wavelengths can be found in Appendix A, Figures A3–A5.

3.3. Intra-Group Analysis

Even though human eyes are most sensitive at 555 nm [42,43] and have shown the capability to differentiate between the extremes of the FSPC (e.g., I vs. VI), results from this study show that human visual evaluation struggled to differentiate between skin types that are more similar on the FSPC scale. As shown in Figure 7a, human FSPC evaluation showed significant differentiation between darker skin types (V and VI) and lighter skin types (I, II, and III) at 560 nm, 585 nm, and 645 nm. However, human eyes struggled to distinguish the finer differences among more similar skin types (i.e., I vs. II, II vs. III, etc.)

Compared to human evaluation, the non-optimized K-means classification (Figure 7b) displays more capability to differentiate skin types at 485 nm and 535 nm. Yet, it still struggled to distinguish different skin types, primarily in the Visible and Near-IR spectra. It is important to note that all K-Means classification methods, optimized or not, do not provide any one-to-one matching for their groupings to a specific FSPC category. Hence, no direct comparison between any two classification results can be conducted.

As described in Section 3.1 and shown in Table 2, K-means$_{410–535}$ showed the same number of multi-participant clusters compared to human evaluation ($k = 6$). In contrast, all other K-means classifications resulted in at least one single-participant group. This observation suggests that K-means$_{410–535}$ might share a similar classifying scheme as human

evaluation whereas other K-means approaches do not. However, there is a discrepancy in the distribution of participants within those six groups, indicating that K-means$_{410–535}$ and human evaluation may be using different grouping criteria. Previous research and the results of this study suggest that human evaluations rely specifically on a narrow bandwidth of light (560–645 nm) to differentiate skin phototypes, whereas K-means$_{410–535}$ relies on a set of shorter wavelengths. When evaluated based on the highest percentage of possible differences among the skin type groups, the K-means$_{730–940}$ method contains the most differentiable intra-grouping results (810–940 nm) among all K-means methods despite presenting an outlier group. However, this differentiation may be more representative of skin temperature, rather than phototype due to the role of temperature in IR wavelength absorption. Even though a comparison of direct grouping results is not achievable in this study, Figure 7 illustrates the resolution of each approach to classify skin phototypes.

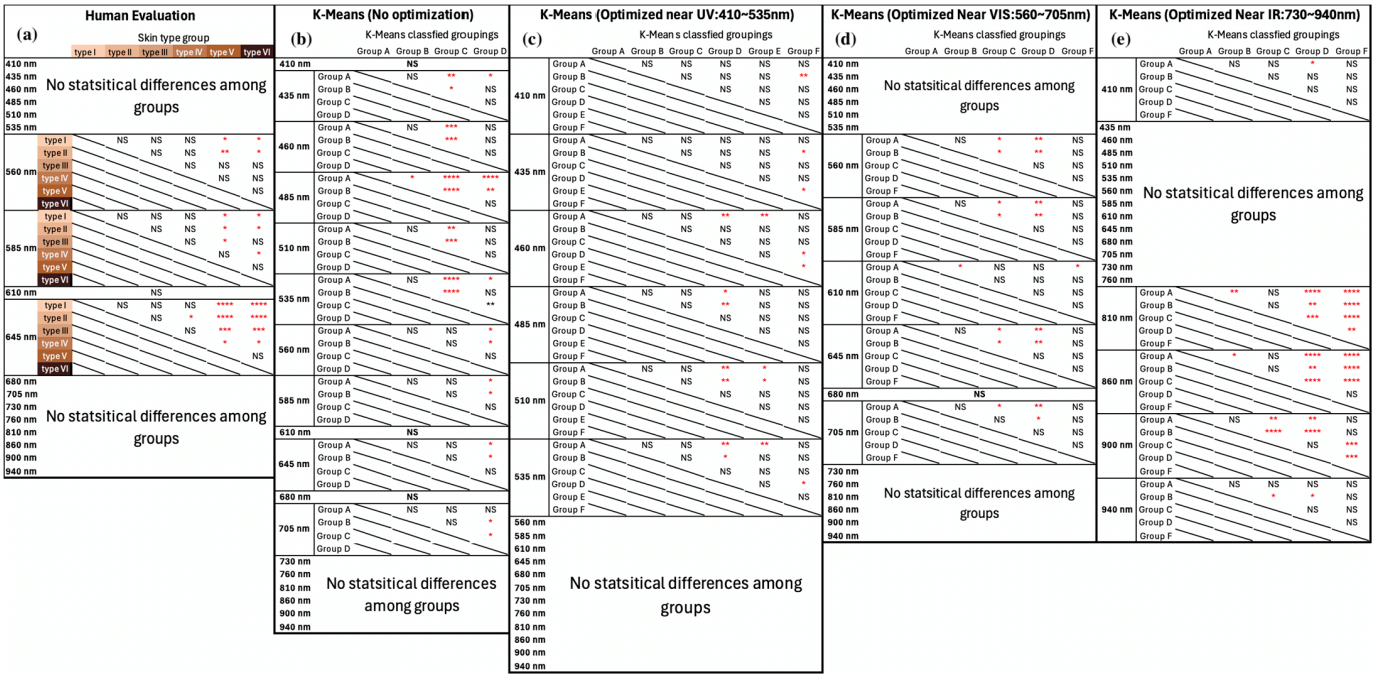

Figure 7. Table of statistical differences for intra-grouping pairwise comparison results at various wavelengths under different classification methods. (**a**) human FSPC classification method, (**b**) K-means$_{410–940}$, (**c**) K-means$_{410–535}$, (**d**) K-means$_{560–705}$, (**e**) K-means$_{730–940}$. Colors in (**a**) represent Fitzpatrick skin type scales I–VI. NS: no statistical difference, *: $p < 0.05$, **: $p < 0.01$, ***: $p < 0.001$, ****: $p < 0.0001$. All statistical tests excluded single-participant groupings. All intra-group level statistical values across different wavelengths can be found in Appendix A, Figures A1–A5.

In summary, K-means classification with optimization offers more customizable, quantifiable, and reproducible skin type classification based on skin optical measurements. However, this study is not without its limitations. For example, this study involved culturally diverse subject groups, but the sample size of the collection is limited and may not represent the full skin optics range present in the human population. Moreover, the sensors used to measure skin optics are not uniformly sensitive across the bandwidth tested. The Near-UV-A and lower visible spectrum wavelengths exhibited greater overall signal power than the other wavelengths tested, which could skew the weightings of these data in the clustering algorithms. Normalization procedures were implemented on each wavelength to reduce the weighting effects. Nevertheless, some effect of this weighting may have persisted in the final dataset, possibly masking finer differences between subjects difficult to detect due to the low signal-to-noise ratio for the channels with lower intensity. A related limitation is that K-means applies the same weighting factor to each wavelength and thus may not fully capture the varying skin optical properties at different wavelengths that drive

skin type differentiation. The algorithm itself is also sensitive to the presence of outliers, the initial location of the centroids, and the uncertainty of optimal cluster numbers. Lastly, the 18 wavelengths sampled across 390–960 nm were not equally distributed (i.e., sampling intervals were non-uniform between wavelengths). These peak sensitivities are based on the bandpass filters designed by the manufacturer of the photodiodes selected for this study. It is possible that different sampling intervals or higher wavelength resolution could affect the results of this study.

Future work should seek to verify these results with broadened light spectra. Due to hardware limitations and participant safety, this study only utilized light in the Near-UV-A spectrum. This light may not share the same optical characteristics of light in the UV-B and UV-A spectra, which hold more clinical relevance for sunburn sensitivity, skin cancer risk, etc. Future work should also seek to verify these results with an increased sample size. A larger dataset would be advantageous for broadening the skin types observed and achieving a normal distribution in the dataset, allowing the use of ANOVA comparisons rather than the less statistically powerful Kruskal–Wallis, as was sometimes required for the present dataset. These factors will also help reduce the chances of single-participant groups in the results. Future work could also explore the use of more complex centroid seed functions (e.g., nonlinear), which might achieve better grouping results by narrowing the search space. Lastly, the results of this study suggest that $k = 6$ may not be the optimal target number of clusters. Future studies could benefit by including techniques such as the elbow method to investigate optimal cluster numbers.

4. Conclusions

This study presented empirical evidence showing that the combined sensor and K-means classification approach can be utilized for skin phototype classification. This method provides advantages over the conventionally used Fitzpatrick Skin Phototype Classification, including better differentiation power and the ability to optimize differentiation at specific bandwidths of interest. The K-means classification methods showed quantifiable and reproducible grouping results that can be segmentally applied to the 410–940 nm spectrum with various medical application focuses.

Author Contributions: X.Y. collected and analyzed data, designed and wrote the analysis software, and prepared the manuscript. M.A.M. designed the experiment, developed the optical sensor software, collected participant data, and reviewed and edited the manuscript. K.G.O. aided in experimental design, aided in analysis approach design, and reviewed and edited the manuscript. All authors have read and agreed to the published version of the manuscript.

Funding: Research reported in this publication was supported by the National Center For Advancing Translational Sciences of the National Institutes of Health under Award Number R41TR004320-01. The content is solely the responsibility of the authors and does not necessarily represent the official views of the National Institutes of Health.

Institutional Review Board Statement: This study was conducted in accordance with the Declaration of Helsinki and approved by the Institutional Review Board at the University of Oregon (STUDY00000643).

Informed Consent Statement: Informed consent was obtained from all subjects involved in this study as approved by the University of Oregon Institutional Review Board. All procedures conformed to the Declaration of Helsinki.

Data Availability Statement: This study's raw data and statistical analysis can be provided upon reasonable request to the authors and in compliance with the NIH guidelines for data sharing.

Acknowledgments: The authors would like to thank Zachary Pennel for his assistance in collecting the data.

Conflicts of Interest: K.G.O. and M.A.M. are affiliated with Penderia Technologies, which is a co-inventor of the technology described in this paper.

Appendix A

Human Evaluation							
Group-wise comparison	Pairwise Comparison						
		type I	type II	type III	type IV	type V	type VI
410 nm ANOVA P = 0.3127	type I		0.4657	0.8952	0.8608	0.992	0.2911
	type II			0.9684	0.9809	0.8028	0.9994
	type III				>0.9999	0.9964	0.8723
	type IV					0.9923	0.905
	type V						0.6118
	type VI						
435 nm K-W P = 0.1457	type I		>0.9999	>0.9999	0.9626	0.8519	0.4657
	type II			>0.9999	>0.9999	>0.9999	>0.9999
	type III				>0.9999	>0.9999	>0.9999
	type IV					>0.9999	>0.9999
	type V						>0.9999
	type VI						
460 nm K-W P=0.2135	type I		>0.9999	>0.9999	>0.9999	>0.9999	>0.9999
	type II			>0.9999	>0.9999	>0.9999	>0.9999
	type III				0.5106	0.2661	>0.9999
	type IV					>0.9999	>0.9999
	type V						>0.9999
	type VI						
485 nm ANOVA P=0.1926	type I		0.9966	0.9334	0.8687	0.7444	>0.9999
	type II			0.9971	0.6107	0.459	0.9981
	type III				0.3434	0.2312	0.9477
	type IV					0.9998	0.8447
	type V						0.7129
	type VI						
510 nm ANOVA P=0.1564	type I		0.9997	0.8743	0.8486	0.7068	>0.9999
	type II			0.9616	0.695	0.5307	0.9975
	type III				0.2443	0.1521	0.8012
	type IV					0.9998	0.911
	type V						0.7946
	type VI						
535 nm K-W P=0.2048	type I		>0.9999	>0.9999	>0.9999	>0.9999	>0.9999
	type II			>0.9999	>0.9999	>0.9999	>0.9999
	type III				0.4462	0.3224	>0.9999
	type IV					>0.9999	>0.9999
	type V						>0.9999
	type VI						
560 nm K-W P=0.0004	type I		>0.9999	>0.9999	>0.9999	0.0127	0.0388
	type II			>0.9999	>0.9999	0.0075	0.0239
	type III				>0.9999	0.1137	0.285
	type IV					0.7076	>0.9999
	type V						>0.9999
	type VI						
585 nm K-W P=0.0003	type I		>0.9999	>0.9999	>0.9999	0.0114	0.0351
	type II			>0.9999	>0.9999	0.0122	0.0373
	type III				>0.9999	0.0445	0.1218
	type IV					>0.9999	>0.9999
	type V						>0.9999
	type VI						
610 nm K-W P=0.6359	type I		>0.9999	>0.9999	>0.9999	>0.9999	>0.9999
	type II			>0.9999	>0.9999	>0.9999	>0.9999
	type III				>0.9999	>0.9999	>0.9999
	type IV					>0.9999	>0.9999
	type V						>0.9999
	type VI						
645 nm ANOVA P<0.0001	type I		0.999	0.9759	0.1027	<0.0001	<0.0001
	type II			0.8775	0.048	<0.0001	<0.0001
	type III				0.3645	0.0001	0.0004
	type IV					0.0185	0.0492
	type V						0.9977
	type VI						
680 nm ANOVA 0.3761	type I		>0.9999	>0.9999	0.9743	0.7869	0.9734
	type II			>0.9999	0.9842	0.7441	0.9836
	type III				0.9477	0.8537	0.9463
	type IV					0.3534	>0.9999
	type V						0.3506
	type VI						
705 nm ANOVA P=0.0106	type I		>0.9999	>0.9999	0.9995	0.1629	0.078
	type II			>0.9999	0.9989	0.145	0.0684
	type III				0.9977	0.1288	0.06
	type IV					0.2785	0.1442
	type V						0.9989
	type VI						
730 nm K-W P=0.3250	type I		>0.9999	>0.9999	>0.9999	>0.9999	>0.9999
	type II			>0.9999	>0.9999	>0.9999	>0.9999
	type III				>0.9999	>0.9999	>0.9999
	type IV					>0.9999	>0.9999
	type V						0.4119
	type VI						
760 nm K-W P=0.1350	type I		>0.9999	>0.9999	>0.9999	0.6791	>0.9999
	type II			>0.9999	>0.9999	>0.9999	>0.9999
	type III				>0.9999	>0.9999	>0.9999
	type IV					0.3957	>0.9999
	type V						0.3121
	type VI						
810 nm ANOVA P=0.6148	type I		0.8755	0.997	0.9997	0.9932	0.9905
	type II			0.6269	0.7309	0.9933	0.9953
	type III				>0.9999	0.9081	0.893
	type IV					0.9564	0.9467
	type V						>0.9999
	type VI						
860 nm ANOVA P=0.4572	type I		0.814	0.9935	0.9983	0.9645	0.9995
	type II			0.4936	0.5749	0.9977	0.9372
	type III				>0.9999	0.7564	0.9516
	type IV					0.8259	0.9762
	type V						0.9963
	type VI						
900 nm K-W P=0.4243	type I		>0.9999	>0.9999	>0.9999	>0.9999	>0.9999
	type II			>0.9999	>0.9999	>0.9999	>0.9999
	type III				>0.9999	>0.9999	>0.9999
	type IV					>0.9999	>0.9999
	type V						0.6295
	type VI						
940 nm ANOVA P=0.7773	type I		0.9991	>0.9999	0.9548	>0.9999	0.9907
	type II			0.998	0.8263	0.9935	>0.9999
	type III				0.9668	>0.9999	0.9856
	type IV					0.9836	0.7036
	type V						0.9696
	type VI						

Figure A1. Groupwise (leftmost column) and pairwise (columns 2–8) comparison analysis results with *p*-value listed of human evaluation grouping results. (K–W: Kruskal–Wallis test). Red font denotes statistical significance.

K-means 410 - 940							
		Pairwise Comparison					
Group-wise comparison		Group A (N =3)	Group B (N = 9)	Group C (N = 12)	Group D (N = 4)	Group E (N = 1)	Group F (N = 1)
410 nm K-W P = 0.6782	Group A		>0.9999	>0.9999	>0.9999		
	Group B			>0.9999	>0.9999		
	Group C				>0.9999		
	Group D						
	Group E						
	Group F						
435 nm ANOVA P = 0.0020	Group A		0.4908	0.0066	0.0329		
	Group B			0.0205	0.1634		
	Group C				0.9983		
	Group D						
	Group E						
	Group F						
460 nm K-W P<0.0001	Group A		>0.9999	0.0007	0.2795		
	Group B			0.0004	>0.9999		
	Group C				0.552		
	Group D						
	Group E						
	Group F						
485 nm ANOVA P<0.0001	Group A		0.0207	<0.0001	<0.0001		
	Group B			<0.0001	0.0042		
	Group C				0.7493		
	Group D						
	Group E						
	Group F						
510 nm K-W P<0.0001	Group A		>0.9999	0.001	0.3008		
	Group B			0.0005	>0.9999		
	Group C				0.6362		
	Group D						
	Group E						
	Group F						
535 nm ANOVA P<0.0001	Group A		0.1951	<0.0001	0.0187		
	Group B			<0.0001	0.3046		
	Group C				0.0063		
	Group D						
	Group E						
	Group F						
560 nm K-W P=0.0074	Group A		>0.9999	>0.9999	0.0168		
	Group B			>0.9999	0.0121		
	Group C				0.0839		
	Group D						
	Group E						
	Group F						
585 nm K-W P=0.0070	Group A		>0.9999	>0.9999	0.0159		
	Group B			>0.9999	0.0112		
	Group C				0.0769		
	Group D						
	Group E						
	Group F						
610 nm ANOVA P=0.2253	Group A		0.9974	0.9918	0.4522		
	Group B			0.8941	0.1752		
	Group C				0.3613		
	Group D						
	Group E						
	Group F						
645 nm K-W P=0.0179	Group A		>0.9999	>0.9999	0.0317		
	Group B			>0.9999	0.0315		
	Group C				0.1252		
	Group D						
	Group E						
	Group F						
680 nm K-W P=0.1793	Group A		>0.9999	>0.9999	>0.9999		
	Group B			>0.9999	0.216		
	Group C				>0.9999		
	Group D						
	Group E						
	Group F						
705 nm K-W P=0.0267	Group A		>0.9999	>0.9999	0.1033		
	Group B			>0.9999	0.0376		
	Group C				0.0415		
	Group D						
	Group E						
	Group F						
730 nm ANOVA P=0.3293	Group A		0.8659	0.995	0.9175		
	Group B			0.4414	0.3594		
	Group C				0.9372		
	Group D						
	Group E						
	Group F						
760 nm K-W P=0.3594	Group A		>0.9999	>0.9999	>0.9999		
	Group B			0.8786	0.9847		
	Group C				0.9999		
	Group D						
	Group E						
	Group F						
810 nm K-W P=0.2938	Group A		>0.9999	>0.9999	>0.9999		
	Group B			0.6918	>0.9999		
	Group C				0.8641		
	Group D						
	Group E						
	Group F						
860 nm ANOVA P=0.1931	Group A		0.9782	0.8943	0.7917		
	Group B			0.3804	0.8821		
	Group C				0.2118		
	Group D						
	Group E						
	Group F						
900 nm ANOVA P=0.8274	Group A		0.7907	0.9139	0.9628		
	Group B			0.9694	0.9748		
	Group C				0.9997		
	Group D						
	Group E						
	Group F						
940 nm ANOVA P=0.7395	Group A		0.9849	0.9904	0.9792		
	Group B			0.7683	0.9995		
	Group C				0.8287		
	Group D						
	Group E						
	Group F						

Figure A2. Groupwise (leftmost column) and pairwise (columns 2–8) comparison analysis results with *p*-value listed of K-means$_{410–940}$ grouping results. (K–W: Kruskal–Wallis test). Red font denotes statistical significance.

K-means 410-535							
		Pairwise Comparsion					
Group-wise comparison		Group A (N = 3)	Group B (N = 5)	Group C (N = 6)	Group D (N = 10)	Group E (N = 2)	Group F (N = 4)
410 nm K-W P = 0.0045	Group A		0.3027	>0.9999	>0.9999	>0.9999	>0.9999
	Group B			0.1116	0.3763	0.4321	0.0014
	Group C				>0.9999	>0.9999	>0.9999
	Group D					>0.9999	0.2727
	Group E						>0.9999
	Group F						
435 nm K-W P = 0.0019	Group A		0.0801	>0.9999	0.389	0.1016	>0.9999
	Group B			>0.9999	>0.9999	>0.9999	0.0176
	Group C				>0.9999	>0.9999	0.8188
	Group D					>0.9999	0.0984
	Group E						0.0381
	Group F						
460 nm K-W P<0.0001	Group A		>0.9999	0.451	0.0031	0.0093	>0.9999
	Group B			>0.9999	0.0517	0.0951	>0.9999
	Group C				>0.9999	0.771	>0.9999
	Group D					>0.9999	0.0139
	Group E						0.0343
	Group F						
485 nm K-W P=0.0003	Group A		>0.9999	0.19	0.0105	0.0645	>0.9999
	Group B			0.293	0.0088	0.1045	>0.9999
	Group C				>0.9999	>0.9999	>0.9999
	Group D					>0.9999	0.2851
	Group E						0.6269
	Group F						
510 nm K-W P<0.0001	Group A		>0.9999	0.4339	0.0045	0.0107	>0.9999
	Group B			>0.9999	0.0076	0.0266	>0.9999
	Group C				>0.9999	0.8777	>0.9999
	Group D					>0.9999	0.1323
	Group E						0.1359
	Group F						
535 nm K-W P<0.0001	Group A		>0.9999	0.4513	0.0031	0.0093	>0.9999
	Group B			>0.9999	0.0196	0.0526	>0.9999
	Group C				>0.9999	0.7714	>0.9999
	Group D					>0.9999	0.0437
	Group E						0.072
	Group F						
560 nm K-W P=0.4665	Group A		>0.9999	0.5596	>0.9999	>0.9999	>0.9999
	Group B			>0.9999	>0.9999	>0.9999	>0.9999
	Group C				>0.9999	>0.9999	>0.9999
	Group D					>0.9999	>0.9999
	Group E						>0.9999
	Group F						
585 nm K-W P=0.3906	Group A		>0.9999	0.4932	>0.9999	>0.9999	>0.9999
	Group B			>0.9999	>0.9999	>0.9999	>0.9999
	Group C				>0.9999	>0.9999	>0.9999
	Group D					>0.9999	>0.9999
	Group E						>0.9999
	Group F						
610 nm K-W P=0.4410	Group A		>0.9999	>0.9999	>0.9999	>0.9999	>0.9999
	Group B			>0.9999	>0.9999	0.8596	>0.9999
	Group C				>0.9999	>0.9999	>0.9999
	Group D					>0.9999	>0.9999
	Group E						>0.9999
	Group F						
645 nm K-W P=0.4982	Group A		>0.9999	0.6883	>0.9999	>0.9999	>0.9999
	Group B			>0.9999	>0.9999	>0.9999	>0.9999
	Group C				>0.9999	>0.9999	>0.9999
	Group D					>0.9999	>0.9999
	Group E						>0.9999
	Group F						
680 nm K-W P=0.3844	Group A		>0.9999	>0.9999	>0.9999	>0.9999	>0.9999
	Group B			>0.9999	>0.9999	0.9117	>0.9999
	Group C				>0.9999	>0.9999	>0.9999
	Group D					0.9351	>0.9999
	Group E						>0.9999
	Group F						
705 nm K-W P=0.6943	Group A		>0.9999	>0.9999	>0.9999	>0.9999	>0.9999
	Group B			>0.9999	>0.9999	>0.9999	>0.9999
	Group C				>0.9999	>0.9999	>0.9999
	Group D					>0.9999	>0.9999
	Group E						>0.9999
	Group F						
730 nm K-W P=0.5692	Group A		>0.9999	>0.9999	>0.9999	>0.9999	>0.9999
	Group B			>0.9999	>0.9999	>0.9999	>0.9999
	Group C				>0.9999	>0.9999	>0.9999
	Group D					>0.9999	>0.9999
	Group E						>0.9999
	Group F						
760 nm K-W P=0.3594	Group A		>0.9999	>0.9999	>0.9999	>0.9999	>0.9999
	Group B			>0.9999	>0.9999	>0.9999	>0.9999
	Group C				>0.9999	>0.9999	>0.9999
	Group D					>0.9999	>0.9999
	Group E						>0.9999
	Group F						
810 nm K-W P=0.2989	Group A		>0.9999	>0.9999	>0.9999	>0.9999	>0.9999
	Group B			>0.9999	>0.9999	>0.9999	>0.9999
	Group C				>0.9999	>0.9999	>0.9999
	Group D					>0.9999	0.5511
	Group E						>0.9999
	Group F						
860 nm K-W P=0.2253	Group A		>0.9999	>0.9999	>0.9999	>0.9999	>0.9999
	Group B			>0.9999	>0.9999	>0.9999	>0.9999
	Group C				0.5533	>0.9999	>0.9999
	Group D					>0.9999	0.4831
	Group E						>0.9999
	Group F						
900 nm K-W P=0.1598	Group A		>0.9999	>0.9999	>0.9999	>0.9999	0.5888
	Group B			>0.9999	>0.9999	>0.9999	0.7069
	Group C				>0.9999	>0.9999	0.1123
	Group D					>0.9999	0.7128
	Group E						>0.9999
	Group F						
940 nm K-W P=0.1353	Group A		>0.9999	>0.9999	>0.9999	>0.9999	>0.9999
	Group B			>0.9999	>0.9999	>0.9999	>0.9999
	Group C				>0.9999	>0.9999	0.4177
	Group D					>0.9999	0.3161
	Group E						0.8144
	Group F						

Figure A3. Groupwise (leftmost column) and pairwise (columns 2–8) comparison analysis results with *p*-value listed of K-means$_{410–535}$ grouping results. (K–W: Kruskal–Wallis test). Red font denotes statistical significance.

K-means 560-705							
		Pairwise Comparsion					
Group-wise comparison		Group A (N = 7)	Group B (N = 4)	Group C (N = 13)	Group D (N = 3)	Group E (N = 1)	Group F (N = 2)
410 nm K-W P = 0.1434	Group A		0.4326	0.5463	>0.9999		0.5162
	Group B			>0.9999	>0.9999		>0.9999
	Group C				>0.9999		>0.9999
	Group D						>0.9999
	Group E						
	Group F						
435 nm K-W P = 0.0861	Group A		>0.9999	0.245	0.531		0.2439
	Group B			>0.9999	>0.9999		>0.9999
	Group C				>0.9999		>0.9999
	Group D						>0.9999
	Group E						
	Group F						
460 nm K-W P=0.5711	Group A		>0.9999	>0.9999	>0.9999		>0.9999
	Group B			>0.9999	>0.9999		>0.9999
	Group C				>0.9999		>0.9999
	Group D						>0.9999
	Group E						
	Group F						
485 nm K-W P=0.5005	Group A		>0.9999	>0.9999	>0.9999		>0.9999
	Group B			>0.9999	0.9403		>0.9999
	Group C				>0.9999		>0.9999
	Group D						>0.9999
	Group E						
	Group F						
510 nm K-W P=0.6735	Group A		>0.9999	>0.9999	>0.9999		>0.9999
	Group B			>0.9999	>0.9999		>0.9999
	Group C				>0.9999		>0.9999
	Group D						>0.9999
	Group E						
	Group F						
535 nm K-W P=0.4709	Group A		>0.9999	>0.9999	>0.9999		>0.9999
	Group B			>0.9999	>0.9999		>0.9999
	Group C				>0.9999		>0.9999
	Group D						>0.9999
	Group E						
	Group F						
560 nm K-W P=0.0001	Group A		>0.9999	0.0336	0.0031		0.291
	Group B			0.0337	0.0026		0.1787
	Group C				0.8246		>0.9999
	Group D						>0.9999
	Group E						
	Group F						
585 nm K-W P=0.0001	Group A		>0.9999	0.0397	0.0035		0.2831
	Group B			0.0299	0.0023		0.1506
	Group C				0.8189		>0.9999
	Group D						>0.9999
	Group E						
	Group F						
610 nm K-W P=0.0013	Group A		0.0186	>0.9999	0.124		0.0176
	Group B			0.2561	>0.9999		>0.9999
	Group C				>0.9999		0.1574
	Group D						>0.9999
	Group E						
	Group F						
645 nm K-W P=0.0002	Group A		>0.9999	0.0173	0.0082		0.749
	Group B			0.0226	0.0071		0.4895
	Group C				>0.9999		>0.9999
	Group D						>0.9999
	Group E						
	Group F						
680 nm K-W P=0.0050	Group A		0.1326	>0.9999	>0.9999		0.1226
	Group B			0.0744	>0.9999		>0.9999
	Group C				0.8479		0.0892
	Group D						>0.9999
	Group E						
	Group F						
705 nm K-W P=0.0004	Group A		>0.9999	0.014	0.0051		>0.9999
	Group B			0.0654	0.013		>0.9999
	Group C				>0.9999		>0.9999
	Group D						0.6677
	Group E						
	Group F						
730 nm K-W P=0.0092	Group A		0.1136	>0.9999	>0.9999		0.0528
	Group B			0.2883	>0.9999		>0.9999
	Group C				>0.9999		0.1238
	Group D						>0.9999
	Group E						
	Group F						
760 nm K-W P=0.0230	Group A		0.1364	>0.9999	>0.9999		0.2734
	Group B			0.1238	>0.9999		>0.9999
	Group C				>0.9999		0.2949
	Group D						>0.9999
	Group E						
	Group F						
810 nm K-W P=0.5295	Group A		>0.9999	>0.9999	>0.9999		>0.9999
	Group B			>0.9999	>0.9999		>0.9999
	Group C				>0.9999		>0.9999
	Group D						>0.9999
	Group E						
	Group F						
860 nm K-W P=0.5836	Group A		>0.9999	>0.9999	>0.9999		>0.9999
	Group B			>0.9999	>0.9999		>0.9999
	Group C				>0.9999		>0.9999
	Group D						>0.9999
	Group E						
	Group F						
900 nm K-W P=0.8713	Group A		>0.9999	>0.9999	>0.9999		>0.9999
	Group B			>0.9999	>0.9999		>0.9999
	Group C				>0.9999		>0.9999
	Group D						>0.9999
	Group E						
	Group F						
940 nm K-W P=0.9592	Group A		>0.9999	>0.9999	>0.9999		>0.9999
	Group B			>0.9999	>0.9999		>0.9999
	Group C				>0.9999		>0.9999
	Group D						>0.9999
	Group E						
	Group F						

Figure A4. Groupwise (leftmost column) and pairwise (columns 2–8) comparison analysis results with *p*-value listed of K-means$_{560–705}$ grouping results. (K–W: Kruskal–Wallis test). Red font denotes statistical significance.

K-means 730-940							
		Pairwise Comparison					
Group-wise comparison		Group A (N = 4)	Group B (N = 11)	Group C (N = 6)	Group D (N = 5)	Group E (N = 1)	Group F (N = 3)
410 nm K-W P = 0.0121	Group A		0.19	0.4216	0.0124		>0.9999
	Group B			>0.9999	>0.9999		>0.9999
	Group C				>0.9999		>0.9999
	Group D						0.145
	Group E						
	Group F						
435 nm ANOVA P = 0.1641	Group A		0.4384	0.8256	0.1796		0.9997
	Group B			0.9671	0.856		0.6808
	Group C				0.6216		0.9398
	Group D						0.3382
	Group E						
	Group F						
460 nm K-W P=0.8290	Group A		>0.9999	>0.9999	>0.9999		>0.9999
	Group B			>0.9999	>0.9999		>0.9999
	Group C				>0.9999		>0.9999
	Group D						>0.9999
	Group E						
	Group F						
485 nm ANOVA P=0.5611	Group A		0.9926	0.5425	0.9711		0.9844
	Group B			0.5858	0.998		0.9994
	Group C				0.8666		0.9116
	Group D						>0.9999
	Group E						
	Group F						
510 nm K-W P=0.8469	Group A		>0.9999	>0.9999	>0.9999		>0.9999
	Group B			>0.9999	>0.9999		>0.9999
	Group C				>0.9999		>0.9999
	Group D						>0.9999
	Group E						
	Group F						
535 nm ANOVA P=0.8705	Group A		0.9113	0.9981	0.9785		0.8908
	Group B			0.974	0.9995		0.9981
	Group C				0.9979		0.9528
	Group D						0.9925
	Group E						
	Group F						
560 nm K-W P=0.2001	Group A		>0.9999	>0.9999	>0.9999		>0.9999
	Group B			>0.9999	>0.9999		0.2158
	Group C				>0.9999		>0.9999
	Group D						>0.9999
	Group E						
	Group F						
585 nm ANOVA P=0.1269	Group A		0.5229	0.8752	0.9973		0.8619
	Group B			0.9715	0.6915		0.1092
	Group C				0.9656		0.3328
	Group D						0.6782
	Group E						
	Group F						
610 nm ANOVA P=0.1074	Group A		0.6366	0.7751	0.9997		0.1922
	Group B			>0.9999	0.4229		0.6328
	Group C				0.6036		0.6417
	Group D						0.1139
	Group E						
	Group F						
645 nm ANOVA P=0.2965	Group A		0.6235	0.9858	>0.9999		0.9848
	Group B			0.8599	0.5691		0.3566
	Group C				0.9849		0.843
	Group D						0.9794
	Group E						
	Group F						
680 nm ANOVA P=0.0215	Group A		0.4562	0.1493	>0.9999		0.0941
	Group B			0.802	0.3374		0.5244
	Group C				0.096		0.9629
	Group D						0.0651
	Group E						
	Group F						
705 nm K-W P=0.0594	Group A		>0.9999	>0.9999	>0.9999		>0.9999
	Group B			>0.9999	0.9534		0.0659
	Group C				>0.9999		0.3561
	Group D						>0.9999
	Group E						
	Group F						
730 nm ANOVA P=0.0416	Group A		0.2601	0.1609	0.9971		0.1188
	Group B			0.9726	0.3759		0.8093
	Group C				0.2339		0.9783
	Group D						0.1698
	Group E						
	Group F						
760 nm ANOVA P=0.0539	Group A		0.2298	0.1317	0.981		0.1477
	Group B			0.9634	0.4807		0.8982
	Group C				0.2857		0.9967
	Group D						0.2902
	Group E						
	Group F						
810 nm ANOVA P<0.0001	Group A		0.0032	0.1516	<0.0001		<0.0001
	Group B			0.4466	0.0015		<0.0001
	Group C				0.0001		<0.0001
	Group D						0.0096
	Group E						
	Group F						
860 nm ANOVA P<0.0001	Group A		0.0492	0.7515	<0.0001		<0.0001
	Group B			0.3583	0.0011		<0.0001
	Group C				<0.0001		<0.0001
	Group D						0.1477
	Group E						
	Group F						
900 nm ANOVA P<0.0001	Group A		0.9866	0.002	0.0013		0.6985
	Group B			<0.0001	<0.0001		0.8215
	Group C				0.9961		0.0002
	Group D						0.0001
	Group E						
	Group F						
940 nm K-W P=0.0065	Group A		>0.9999	0.4524	0.5814		>0.9999
	Group B			0.0212	0.0436		>0.9999
	Group C				>0.9999		>0.9999
	Group D						>0.9999
	Group E						
	Group F						

Figure A5. Groupwise (leftmost column) and pairwise (columns 2–8) comparison analysis results with *p*-value listed of K-means$_{730–940}$ grouping results. (K–W: Kruskal–Wallis test). Red font denotes statistical significance.

References

1. Shope, C.N.; Andrews, L.A.; Neimy, H.; Linkous, C.L.; Khamdan, F.; Lee, L.W. Characterizing Skin Cancer in Transplant Recipients by Fitzpatrick Skin Phototype. *Dermatol. Ther.* **2023**, *13*, 147–154. [CrossRef] [PubMed]
2. Jablonski, N.G. The Evolution of Human Skin Pigmentation Involved the Interactions of Genetic, Environmental, and Cultural Variables. *Pigment Cell Melanoma Res.* **2021**, *34*, 707–729. [CrossRef] [PubMed]
3. Sonenblum, S.E.; Patel, R.; Phrasavath, S.; Xu, S.; Bates-Jensen, B.M. Using Technology to Detect Erythema Across Skin Tones. *Adv. Ski. Wound Care* **2023**, *36*, 524–533. [CrossRef] [PubMed]
4. Monk, E.P. The Unceasing Significance of Colorism: Skin Tone Stratification in the United States. *Daedalus* **2021**, *150*, 76–90. [CrossRef]
5. Mitchell, M.; Wu, S.; Zaldivar, A.; Barnes, P.; Vasserman, L.; Hutchinson, B.; Spitzer, E.; Raji, I.D.; Gebru, T. Model Cards for Model Reporting. In Proceedings of the Conference on Fairness, Accountability, and Transparency, Atlanta, GA, USA, 29–31 January 2019; pp. 220–229.
6. Oliveira, R.; Ferreira, J.; Azevedo, L.F.; Almeida, I.F. An Overview of Methods to Characterize Skin Type: Focus on Visual Rating Scales and Self-Report Instruments. *Cosmetics* **2023**, *10*, 14. [CrossRef]
7. Fitzpatrick, T.B. The Validity and Practicality of Sun-Reactive Skin Types I through VI. *JMMA Dermatol.* **1988**, *124*, 869–871. [CrossRef]
8. Lim, S.S.; Mohammad, T.F.; Kohli, I.; Hamzavi, I.; Rodrigues, M. Optimisation of Skin Phototype Classification. *Pigment Cell Melanoma Res.* **2023**, *36*, 468–471. [CrossRef]
9. Tsai, S.-R.; Hamblin, M.R. Biological Effects and Medical Applications of Infrared Radiation. *J. Photochem. Photobiol. B Biol.* **2017**, *170*, 197–207. [CrossRef]
10. Ware, O.R.; Dawson, J.E.; Shinohara, M.M.; Taylor, S.C. Racial Limitations of Fitzpatrick Skin Type. *Cutis* **2020**, *105*, 77–80.
11. Clement, M.; Daniel, G.; Trelles, M. Optimising the Design of a Broad-band Light Source for the Treatment of Skin. *J. Cosmet. Laser Ther.* **2005**, *7*, 177–189. [CrossRef]
12. Shi, C.; Goodall, M.; Dumville, J.; Hill, J.; Norman, G.; Hamer, O.; Clegg, A.; Watkins, C.L.; Georgiou, G.; Hodkinson, A.; et al. The Accuracy of Pulse Oximetry in Measuring Oxygen Saturation by Levels of Skin Pigmentation: A Systematic Review and Meta-Analysis. *BMC Med.* **2022**, *20*, 267. [CrossRef] [PubMed]
13. Jamali, H.; Castillo, L.T.; Morgan, C.C.; Coult, J.; Muhammad, J.L.; Osobamiro, O.O.; Parsons, E.C.; Adamson, R. Racial Disparity in Oxygen Saturation Measurements by Pulse Oximetry: Evidence and Implications. *Ann. ATS* **2022**, *19*, 1951–1964. [CrossRef] [PubMed]
14. Sjoding, M.W.; Dickson, R.P.; Iwashyna, T.J.; Gay, S.E.; Valley, T.S. Racial Bias in Pulse Oximetry Measurement. *New Engl. J. Med.* **2020**, *383*, 2477–2478. [CrossRef] [PubMed]
15. Johnson, J.; Johnson, A.R.; Andersen, C.A.; Kelso, M.R.; Oropallo, A.R.; Serena, T.E. Skin Pigmentation Impacts the Clinical Diagnosis of Wound Infection: Imaging of Bacterial Burden to Overcome Diagnostic Limitations. *J. Racial Ethn. Health Disparities* **2024**, *11*, 1045–1055. [CrossRef]
16. Narla, S.; Heath, C.R.; Alexis, A.; Silverberg, J.I. Racial Disparities in Dermatology. *Arch. Dermatol. Res.* **2022**, *315*, 1215–1223. [CrossRef]
17. Linde, K.; Wright, C.Y.; Du Plessis, J.L. Subjective and Objective Skin Colour of a Farmworker Group in the Limpopo Province, South Africa. *Ski. Res. Technol.* **2020**, *26*, 923–931. [CrossRef]
18. Reeder, A.I.; Hammond, V.A.; Gray, A.R. Questionnaire Items to Assess Skin Color and Erythemal Sensitivity: Reliability, Validity, and "the Dark Shift". *Cancer Epidemiol. Biomark. Prev.* **2010**, *19*, 1167–1173. [CrossRef]
19. Krutmann, J.; Piquero-Casals, J.; Morgado-Carrasco, D.; Granger, C.; Trullàs, C.; Passeron, T.; Lim, H.W. Photoprotection for People with Skin of Colour: Needs and Strategies. *Br. J. Dermatol.* **2023**, *188*, 168–175. [CrossRef]
20. Xiao, K.; Yates, J.M.; Zardawi, F.; Sueeprasan, S.; Liao, N.; Gill, L.; Li, C.; Wuerger, S. Characterising the Variations in Ethnic Skin Colours: A New Calibrated Data Base for Human Skin. *Ski. Res. Technol.* **2017**, *23*, 21–29. [CrossRef]
21. Everett, J.S.; Budescu, M.; Sommers, M.S. Making Sense of Skin Color in Clinical Care. *Clin. Nurs. Res.* **2012**, *21*, 495–516. [CrossRef]
22. He, S.Y.; McCulloch, C.E.; Boscardin, W.J.; Chren, M.-M.; Linos, E.; Arron, S.T. Self-Reported Pigmentary Phenotypes and Race Are Significant but Incomplete Predictors of Fitzpatrick Skin Phototype in an Ethnically Diverse Population. *J. Am. Acad. Dermatol.* **2014**, *71*, 731–737. [CrossRef] [PubMed]
23. Ly, B.C.K.; Dyer, E.B.; Feig, J.L.; Chien, A.L.; Del Bino, S. Research Techniques Made Simple: Cutaneous Colorimetry: A Reliable Technique for Objective Skin Color Measurement. *J. Investig. Dermatol.* **2020**, *140*, 3–12.e1. [CrossRef] [PubMed]
24. Finlayson, L.; Barnard, I.R.M.; McMillan, L.; Ibbotson, S.H.; Brown, C.T.A.; Eadie, E.; Wood, K. Depth Penetration of Light into Skin as a Function of Wavelength from 200 to 1000 Nm. *Photochem Photobiol.* **2022**, *98*, 974–981. [CrossRef] [PubMed]
25. Ash, C.; Dubec, M.; Donne, K.; Bashford, T. Effect of Wavelength and Beam Width on Penetration in Light-Tissue Interaction Using Computational Methods. *Lasers Med. Sci.* **2017**, *32*, 1909–1918. [CrossRef]
26. Lanzafame, R. Light Dosing and Tissue Penetration: It Is Complicated. *Photobiomodulation Photomed. Laser Surg.* **2020**, *38*, 393–394. [CrossRef] [PubMed]
27. Lister, T.; Wright, P.A.; Chappell, P.H. Optical Properties of Human Skin. *J. Biomed. Opt.* **2012**, *17*, 0909011. [CrossRef]

28. Groh, M.; Badri, O.; Daneshjou, R.; Koochek, A.; Harris, C.; Soenksen, L.R.; Doraiswamy, P.M.; Picard, R. Deep Learning-Aided Decision Support for Diagnosis of Skin Disease across Skin Tones. *Nat. Med.* **2024**, *30*, 573–583. [CrossRef]
29. Gajinov, Z.; Matić, M.; Prćić, S.; Đuran, V. Optical Properties of the Human Skin/Optičke Osobine Ljudske Kože. *Serbian J. Dermatol. Venerol.* **2010**, *2*, 131–136. [CrossRef]
30. Austin, E.; Geisler, A.N.; Nguyen, J.; Kohli, I.; Hamzavi, I.; Lim, H.W.; Jagdeo, J. Visible Light. Part I: Properties and Cutaneous Effects of Visible Light. *J. Am. Acad. Dermatol.* **2021**, *84*, 1219–1231. [CrossRef]
31. Anderson, R.R.; Parrish, J.A. The Optics of Human Skin. *J. Investig. Dermatol.* **1981**, *77*, 13–19. [CrossRef]
32. Moreiras, H.; Seabra, M.C.; Barral, D.C. Melanin Transfer in the Epidermis: The Pursuit of Skin Pigmentation Control Mechanisms. *Int. J. Mol. Sci.* **2021**, *22*, 4466. [CrossRef] [PubMed]
33. Passeron, T.; Lim, H.W.; Goh, C.-L.; Kang, H.Y.; Ly, F.; Morita, A.; Ocampo Candiani, J.; Puig, S.; Schalka, S.; Wei, L.; et al. Photoprotection According to Skin Phototype and Dermatoses: Practical Recommendations from an Expert Panel. *Acad. Dermatol. Venereol.* **2021**, *35*, 1460–1469. [CrossRef] [PubMed]
34. Ito, S.; Wakamatsu, K.; Ozeki, H. Chemical Analysis of Melanins and Its Application to the Study of the Regulation of Melanogenesis. *Pigment. Cell Res.* **2000**, *13*, 103–109. [CrossRef] [PubMed]
35. Brenner, M.; Hearing, V.J. The Protective Role of Melanin Against UV Damage in Human Skin †. *Photochem. Photobiol.* **2008**, *84*, 539–549. [CrossRef]
36. Setchfield, K.; Gorman, A.; Simpson, A.H.R.W.; Somekh, M.G.; Wright, A.J. Effect of Skin Color on Optical Properties and the Implications for Medical Optical Technologies: A Review. *J. Biomed. Opt.* **2024**, *29*, 010901. [CrossRef]
37. Sinaga, K.P.; Yang, M.-S. Unsupervised K-Means Clustering Algorithm. *IEEE Access* **2020**, *8*, 80716–80727. [CrossRef]
38. Al-Mohair, H.K.; Mohamad Saleh, J.; Suandi, S.A. Hybrid Human Skin Detection Using Neural Network and K-Means Clustering Technique. *Appl. Soft Comput.* **2015**, *33*, 337–347. [CrossRef]
39. Anas, M.; Gupta, R.K.; Ahmad, D.S. Skin Cancer Classification Using K-Means Clustering. *Int. J. Tech. Res. Appl.* **2017**, *5*, 62–65.
40. Starczewski, A.; Krzyżak, A. Performance Evaluation of the Silhouette Index. In Proceedings of the Artificial Intelligence and Soft Computing: 14th International Conference, ICAISC 2015, Zakopane, Poland, 14–18 June 2015; Lecture Notes in Computer Science, Rutkowski, L., Korytkowski, M., Scherer, R., Tadeusiewicz, R., Zadeh, L., Zurada, J., Eds.; Springer: Cham, Switzerland, 2015; Volume 9120. [CrossRef]
41. Smith, W.J. *Modern Optical Engineering: The Design of Optical Systems*, 3rd ed.; McGraw Hill: New York, NY, USA, 2000; ISBN 978-0-07-136360-0.
42. Konatham, S.; Martín-Torres, J.; Zorzano, M.-P. The Impact of the Spectral Radiation Environment on the Maximum Absorption Wavelengths of Human Vision and Other Species. *Life* **2021**, *11*, 1337. [CrossRef]
43. Delgado-Bonal, A.; Martín-Torres, J. Human Vision Is Determined Based on Information Theory. *Sci. Rep.* **2016**, *6*, 36038. [CrossRef]
44. D'Orazio, J.; Jarrett, S.; Amaro-Ortiz, A.; Scott, T. UV Radiation and the Skin. *Int. J. Mol. Sci.* **2013**, *14*, 12222–12248. [CrossRef] [PubMed]
45. Kim, J.S.; Park, S.W.; Choi, T.H.; Kim, N.G.; Lee, K.S.; Kim, J.R.; Lee, S.-I.; Kang, D.; Han, K.H.; Son, D.G.; et al. The Evaluation of Relevant Factors Influencing Skin Graft Changes in Color Over Time: The Color of Skin Graft. *Dermatol. Surg.* **2007**, *34*, 32–39. [CrossRef] [PubMed]